Patterns of cell death triggered in two different cell lines by HypF-N prefibrillar aggregates

Monica Bucciantini,* Stefania Rigacci,* Andrea Berti,* Laura Pieri,* Cristina Cecchi,* Daniele Nosi,[†] Lucia Formigli,[†] Fabrizio Chiti,* and Massimo Stefani*,[‡]

*Department of Biochemical Sciences, [†]Department of Anatomy, Histology and Forensic Medicine, [‡]Center of Excellence for Molecular and Clinical Studies on Chronic, Inflammatory, Degenerative and Tumoural Diseases for the Development of New Therapies, University of Florence, Florence, Italy

Monica Bucciantini and Stefania Rigacci contributed equally to this work.

Corresponding author: Massimo Stefani, Department of Biochemical Sciences, Viale Morgagni 50, 50134 Florence, Italy. E-mail: stefani@scibio.unifi.it

ABSTRACT

The finding that aggregates of disease-unrelated proteins can induce cell death indicates that proteins may act as potential toxins. Cells experiencing toxic protein aggregates often display modifications of the redox status and ion balance, eventually leading to apoptosis; however, in some cases, tissue and cultured cell types die with features of necrosis. To elucidate the pathways leading to such different outcomes, we studied the biochemical features of death in H-END and NIH/3T3 cells exposed to prefibrillar aggregates of a disease-unrelated protein. The two types of cells died by apoptosis and necrosis, respectively. The pattern of caspase and proapoptotic factor activation was investigated together with the extent of mitochondria impairment and the energy load in either cell line. Our data depict a scenario where the events related to the extrinsic pathway of apoptosis are the same in the two cell lines, the difference in the final outcome being related to the extent of mitochondria derangement, possibly due to the different ability of the cells to counteract ion homeostasis impairment.

Key words: protein aggregation • aggregate toxicity • amyloid fibrils • cell apoptosis • cell necrosis

T he main hallmark of a number of sporadic or familial degenerative diseases, either systemic or affecting the central nervous system (CNS), is the presence, in the affected organs and tissues, of intracellular or extracellular deposits of fibrillar appearance (amyloid fibrils). These deposits result from the aggregation of one out of a limited number of peptides or proteins, each specific of a particular disease (1) after mutations, overexpression, chemical modifications, or impairment of cellular components of the folding quality control (1). Presently, there is growing interest in improving our knowledge of the molecular and biochemical basis of protein misfolding and aggregation as well as of aggregate toxicity to living systems. Such knowledge could suggest clues for the development of therapeutic strategies to

treat pathologies with dramatic social impact, such as Alzheimer's disease (AD) and Parkinson's disease, senile systemic amyloidosis, AA and AL amyloidosis, and type II diabetes mellitus (2–4).

It is currently believed that peptide and protein aggregates are the main culprit of cell impairment eventually leading to cell death with memory loss and cognitive impairment when aggregation occurs in the brain. However, the type(s) of aggregates endowed with the highest toxicity and giving rise to the onset of neuropathic diseases are still matter of debate. An increasing body of evidence supports the idea that the causative agents of neuropathic protein deposition diseases are oligomeric assemblies (prefibrillar aggregates) preceding the appearance of mature fibrils (5–8). In addition, it has been shown that prefibrillar aggregates of differing polypeptide chains share basic structural features, and this "toxic fold" appears to be associated with the impairment and death of exposed cells (5). Toxic prefibrillar aggregates share also common mechanisms of cytotoxicity, where early modifications of the intracellular redox status and ion homeostasis appear to play a key role (1, 9–13), although, in some cases, such as the neurodegenerative diseases caused by triplet expansions, other mechanisms of toxicity have been reported (14).

It is well known that extensive death of specific neuronal populations occurs either physiologically, as during embryogenesis or after trauma, and in neurodegenerative diseases (15); however, even in this case, the pathways eventually leading to cell death are poorly understood at the cellular and biochemical levels. In most cases, the final outcome is cell death by apoptosis, although necrotic features in dead cells have also been shown (16–19). In addition, recently, a new type of programmed cell death induced by oxidative stress with glutathione depletion, referred to as oxytosis, has been reported (20). Moreover, under pathological conditions, apoptosis and nonapoptotic death paradigms often appear interwined, suggesting that in vivo cells can use diverging execution pathways (21).

The perspective in the research on the molecular basis of protein aggregation and aggregate toxicity has changed since 1998, when it was first shown that the ability to misfold and aggregate is not a peculiar property associated with the specific amino acid sequences of the proteins and peptides implicated in protein deposition diseases (1); rather, it appears as an inherent property of the polypeptide backbone of any peptide sequence (including amino acid homopolymers) (22). Later on, it has been shown that even aggregates of proteins and peptides not associated with any amyloid disease display toxic effects on cultured cells (6, 23–25) and whole animals (S. Baglioni and M. Stefani, unpublished observations).

This body of data led us to consider protein aggregation and aggregate toxicity as generic properties of polypeptide chains not associated with specific amino acid sequences. Hence, amyloid diseases are now considered pathological states arising when a natural polypeptide chain becomes organized so as to assemble into a generic polymer structure rather than folding in the biologically active three-dimensional conformation encoded into its amino acid sequence (22). These data led us to suggest that a higher number of degenerative diseases than presently known might follow the deposition of proteins and peptides presently considered not associated to disease (1) and that aggregation of specific proteins may be endowed with physiological significance in biological systems (26).

We have previously reported that prefibrillar aggregates, but not mature fibrils, of a protein unrelated with any disease, the N-terminal domain of the hydrogenase maturation factor HypF

(HypF-N), are able to enter into NIH/3T3 cells after incubation in the culture medium. As a consequence, the cells display impaired viability with early modifications of basic biochemical parameters such as intracellular redox status and free Ca^{2+} (23). In this study, we have investigated the biochemical features of cell death upon exposure to HypF-N toxic prefibrillar aggregates using H-END and NIH/3T3 previously shown to display a different final outcome, apoptosis or necrosis, respectively, upon exposure to toxic amyloid aggregates. In addition, H-END cells are highly sensitive to the toxic effects of the cross-β structure characteristic of aggregates of proteins and peptides such as Aβ peptides and are damaged in cerebral vessels of AD people (reviewed in ref 27).

A better knowledge of the biochemical responses of cells exposed to toxic protein aggregates is of the outmost importance to know what exactly happens in tissues and organs experiencing protein toxic assemblies. It is also mandatory to rationally design molecules and treatments aimed at counteracting the harmful effects of protein aggregates on living systems and at favoring the natural defenses of cells and tissues against them.

MATERIALS AND METHODS

Materials

HypF-N was purified as described previously (28). Ac-LEHD-AMC and cell-permeable Ac-IETD-CHO were from Biosource International; all other caspase substrates and inhibitors were from Biomol Research Laboratories Inc. The Klenow-Frag-EL^{TM} DNA fragmentation detection kit and the annexin V detection kit were from Oncogene Research Products (San Diego, CA). The lipophilic cationic probe 5,5′,6,6′-tetrachloro-1,1′,3,3′-tetraethylbenzimidazol-carbocyanine iodide (JC-1) was from Molecular Probes (Eugene, OR). The ATP assay kit was from Sigma-Aldrich Fine Chemicals Co. (St. Louis, MO). Rabbit anti-Bax polyclonal antibody was from Chemicon International (Temecula, CA); rabbit anti-Bid polyclonal antibody was from Santa Cruz Biotechnology, Inc. (Santa Cruz, CA); and mouse anti-p53 (1C12) monoclonal antibody and rabbit anti-caspase-6 polyclonal antibody were from Cell Signaling Technology (Beverly, MA). Enhanced chemiluminescence detection substrate (ECL) was from Amersham Biosciences (Uppsala, Sweden). Cell culture media, materials for microscopy analysis, and other reagents were from Sigma-Aldrich Fine Chemicals Co. NIH/3T3 murine fibroblasts and H-END murine endothelioma cells (from the laboratory of F. Bussolino, University of Turin, Italy) were routinely cultured in Dulbecco's modified Eagle's medium (DMEM) with 4.5 g/l glucose, containing 10% bovine calf serum (HyClone Lab, Perbio Company, Celbio) or fetal calf serum (Sigma), respectively, unless otherwise stated, and 3.0 mM glutamine in a 5.0% CO_2 humidified environment at 37°C, and 100.0 U/ml penicillin and 100.0 μg/ml streptomycin were added to the media. Cells were used for a maximum of 20 passages.

Formation of prefibrillar aggregates of HypF-N

HypF-N prefibrillar aggregates were obtained by incubating the protein for 48 h at room temperature at a concentration of 0.3 mg/ml in 30% (v/v) trifluoroethanol, 50 mM sodium acetate, 2.0 mM dithiotreitol (DTT), pH 5.5, as previously reported (28). The solution was centrifuged, and the resulting pellet was dried under N_2 to remove the residual solvent, dissolved in phosphate-buffered saline (PBS), and immediately added to the cell culture medium.

Hematoxylin and eosin staining

Cells were plated on glass coverslips and exposed to different final concentrations of HypF-N prefibrillar aggregates added to culture medium. After 24 h, cells were washed twice with PBS, fixed with 2.0% buffered paraformaldheyde for 10 min at room temperature, washed with PBS and with redistilled water, and stained for 5 min in hematoxylin. After additional washings for 5 min with tap water and for 2 min with redistilled water, the coverslips were stained for 2 min in 0.2% eosin; rapidly dipped in 80% ethanol (1 min), 90% ethanol (1 min), and 100% ethanol (1 min) and xylol (5 min); mounted on slides with Canada balsam; and analyzed by light microscopy.

In situ end labeling of nicked DNA

Apoptotic cells were identified by light microscopy after end labeling of DNA fragments by using the Klenow-Frag-EL DNA fragmentation detection kit (ISEL assay) according to the instructions provided by the manufacturer. Briefly, cells were exposed to various concentrations of HypF-N prefibrillar aggregates or to the same amounts of monomeric HypF-N. After 24 h, exposed cells were fixed in 2.0% buffered paraformaldheyde (10 min) and incubated with 20 μg/ml proteinase-K for 5 min at room temperature to remove the excess proteins from the nuclei. Endogenous peroxidase was inactivated by covering the cells with 3.0% H_2O_2 for 5 min at room temperature. Then the cells were incubated with the Klenow fragment of DNA polymerase-I and biotinylated deoxyribonucleotides in a humidified chamber at 37°C for 1.5 h. The reaction was stopped by moving the slides with the adherent cells into the blocking solution (300 mM NaCl, 30 mM sodium citrate) for 15 min at room temperature. After incubation for 10 min with streptavidin-peroxidase, the cells were stained with diaminobenzidine for 10 min at room temperature. Diaminobenzidine reacts with the labeled fragmented DNA of apoptotic cell nuclei, generating a dark brown insoluble chromogen. Counterstaining was performed with methyl green. The number of the cells displaying nuclear staining was determined by counting four different fields each containing ~50 cells.

Annexin V and propidium iodide labeling

Cells undergoing early apoptosis were evidenced by phosphatidylserine (PS) staining using an annexin V detection kit according to the instructions of the manufacturer. Briefly, control cells exposed to 2.0 μM monomeric HypF-N and cells exposed to 2.0 μM HypF-N prefibrillar aggregates were gently detached with 0.25% trypsin in PBS, centrifuged at 1800 rpm for 10 min, and resuspended in DMEM at 10^6 cells/ml. The cells were double-stained with FITC-conjugated annexin V, which binds to PS, while nuclei were stained with propidium iodide. The specimens were analyzed with a Bio-Rad 1024 ES confocal laser scanning microscope (Bio-Rad, Hampstead, UK) with laser beam excitation at 488 and 568 nm wavelengths.

Caspase activity assay

Cells exposed to the HypF-N prefibrillar aggregates were washed twice with PBS and then lysed for 20 min at 0-4°C in 20 mM Tris-HCl buffer, pH 7.4, containing 250 mM NaCl, 2.0 mM EDTA, 0.1% Triton X-100, 5.0 μg/ml aprotinin, 5.0 μg/ml leupeptin, 0.5 mM phenylmethylsulfonylfluoride, 4.0 mM sodium vanadate, and 1.0 mM DTT. The lysis was completed by sonication, and total protein content was determined in the clarified lysates with

the Bradford reagent. Aliquots of total proteins (50 µg for caspase-9 assay, 250 µg for caspase-8 and caspase-3 assays) were diluted in 50 mM HEPES-KOH buffer, pH 7.0, containing 10% glycerol, 0.1% 3-[(3-cholamidopropyl)-dimethylammonio]-1-propane sulfonate, 2.0 mM EDTA, 10 mM DTT. Caspase-9 activity was determined by incubating a protein sample for 2 h at 37°C in the presence of 50 µM Ac-LEHD-AMC (fluorometric substrate; excitation 380 nm, emission 460 nm). Caspase-3 and -8 activities were determined by incubating a protein sample for 4 h at 37°C in the presence of 200 µM Ac-DEVD-pNA and 200 µM Ac-IETD-pNA, respectively, and evaluating sample extinction at 405 nm. To determine nonspecific substrate degradation, the assays were also performed by preincubating total protein samples for 15 min at 37°C with or without the specific caspase inhibitor (100 nM Ac-DEVD-CHO for caspase-3; 50 µM Ac-IETD-CHO for caspase-8; 10 µM Ac-LEHD-CHO for caspase-9) before substrate addition. As a positive control, cells were treated with 2.0 µM staurosporine for 5 h before lysis. In some experiments, cells were pretreated for 2 h with a cell permeable caspase-8 inhibitor (10 µM) before exposure to the prefibrillar aggregates.

Determination of mitochondrial membrane potential in living cells

The change of the mitochondrial membrane potential ($\Delta\Psi_M$) occurring during apoptosis was detected by a fluorescence-based assay. NIH/3T3 and H-END cells were incubated for 10 min at 37°C on coverslips in DMEM containing 5.0 mg/ml of the lipophilic cationic probe JC-1. At hyperpolarized membrane potentials (-140 mV), the dye forms a red fluorescent J-aggregate, whereas at depolarized membrane potentials (-100 mV), it remains in the green fluorescent monomeric form. Before detection, cells were washed in PBS and placed in an open slide-flow loading chamber that was mounted on the stage of a Bio-Rad MRC 1024 ES Confocal Laser Scanning Microscope (CLSM) equipped with a Krypton/Argon (Kr/Ar) laser source. The emitted fluorescence was monitored at 488 and 568 nm with a Nikon plan ApoX60 oil-immersion objective. Series of optical sections (512×512 pixels) were taken trough the depth of cells with a thickness of 1.0 µm at intervals of 0.8 µm. Twenty optical sections for each sample were projected as a single composite image by superimposition.

Intracellular ATP assay

Intracellular ATP was measured by a somatic cell assay kit based on luciferin-luciferase reaction according to the instructions provided by the manufacturer. When ATP is the limiting component in the luciferase reaction, the intensity of the emitted light is proportional to the ATP concentration in the cytosolic extract. Briefly, nonconfluent cells were incubated with 2.0 µM HypF-N prefibrillar aggregates or with the same concentration of monomeric HypF-N as a control in fresh medium. After 24 h, the cells were washed twice with PBS, trypsinized and resuspended in fresh DMEM without phenol red, and supplemented with 10% bovine calf serum. Cells were counted and diluted to a final density of 2×10^5 cells/ml. The ATP content was measured in light intensity using a Berthold Lumat LB 96507 luminometer, and the percent variation was calculated for every cell line with respect to its control.

Western blot analysis

After treatment with 2.0 µM HypF-N prefibrillar aggregates or with 2.0 µM soluble HypF-N as a control, cells were washed twice with PBS and lysed in RIPA buffer [50 mM Tris-HCl buffer,

pH 8.0, 150 mM NaCl, 1.0% (v/v) Nonidet P-40, 0.1% (w/v) SDS, 0.5% (w/v) sodium deoxycholate, 1.0 mM sodium vanadate, 10 μg/ml leupeptin, 20 μg/ml aprotinin, and 1.0 mM PMSF] for 30 min in ice. Protein concentration was determined by the bicinchoninic acid assay. Equal protein amounts were run in SDS-PAGE and transferred to PVDF membranes. Blots were incubated with primary antibodies (anti-Bid 1:500, anti-p53 1:1000, anti-Bax 1:1500, anti-caspase-6 1:500) at 4°C overnight. After being washed, the blots were stained with peroxidase-conjugated secondary antibody and the bands were visualized by ECL. Images were acquired with ChemiDoc apparatus (Bio-Rad), and densitometric analysis of bands was performed using QuantiScan software (Bio-Rad).

RESULTS

HypF-N prefibrillar aggregates induce apoptosis in H-END and necrosis in NIH/3T3 cells

NIH/3T3 and H-END cells were treated for various intervals of time with different concentrations of toxic HypF-N prefibrillar aggregates to test aggregate cytotoxicity and to determine the mode of cell death. Controls were performed by exposing the cells to the same amount of soluble HypF-N (Fig. 1A and D). NIH/3T3 cells exposed for 24 h to 10 μM (monomeric protein concentration) HypF-N prefibrillar aggregates died with necrotic features, such as cellular and nuclear swelling and cytoplasmic vacuolization, as shown by hematoxylin and eosin staining (Fig. 1E and F). In contrast, under the same conditions, H-END cells displayed typical features of apoptosis, such as nuclear condensation, chromatin aggregation, and plasma membrane blebbing (Fig. 1B and C). Apoptotic cells were also recognized on the basis of their characteristic DNA fragmentation by nick-end labeling with the Klenow-FragEl method. This treatment allows easy recognition apoptotic cells by the presence of a dark brown nuclear staining, whereas viable cells appear green or even unstained. Exposed H-END cells displayed oligo-nucleosomal DNA fragmentation (Fig. 2B). No DNA fragmentation was observed in NIH/3T3 cells under the same conditions, although sample counterstaining revealed the presence of cytoplasmic vacuolization (Fig. 2D). No DNA fragmentation was observed in control cells of both lines (Fig. 2A and C).

Figure 2, lower panel, shows the number of apoptotic H-END cells after 24 h exposure as a function of the amount of prefibrillar aggregates added to the culture medium. The percentage of apoptotic nuclei increases with the concentration of prefibrillar HypF-N aggregates, reaching 18% at the highest tested concentration (10 μM). At 24 h of exposure and 2.0 μM concentration of HypF-N aggregates, ~8.0% of the cells showed brown stained nuclei (1.0% in control cells); this concentration was chosen to investigate finely regulated biochemical processes, such as the activation of proapoptotic factors, that could have been obscured by a stronger cell injury.

A key apoptotic event is the modification of the plasma membrane composition, a signal for recognition and engulfment by phagocytes before membrane integrity is compromised (29). A marker for phagocytosis is the exposure of PS, a phospholipid normally found in the inner leaflet of the cell membrane that flips to the outer leaflet during the early stages of apoptosis (29). Annexin V preferentially binds to PS and can be used to detect PS exposure on the external surface of apoptotic cells (30).

H-END and NIH/3T3 cells were exposed for 24 h to 2.0 μM prefibrillar aggregates or to 2.0 μM soluble protein as a control. While control cells displayed no annexin V-FITC binding and an

unaffected plasma membrane (Fig. 3A), exposed H-END cells displayed annexin V positivity as an annular staining of the cell membrane, indicating membrane integrity but PS exposure on the membrane external surface (Fig. 3B). In contrast, in NIH/3T3 cells exposed to the HypF-N aggregates a cytoplasmic staining was observed, suggesting the presence of plasma membrane ruptures as a consequence of necrosis (Fig. 3D). To explain the different effects caused by the exposure to the HypF-N prefibrillar aggregates in H-END and NIH/3T3 cells, the biochemical pathways involved in aggregate toxicity were investigated in more detail.

Caspase activation during H-END and NIH/3T3 cell death

Caspase activity was determined in NIH/3T3 and H-END cells exposed for 5, 8, 16, and 24 h to 2.0 μM HypF-N prefibrillar aggregates or to the soluble protein. In H-END cells exposed for 5, 16, and 24 h to the aggregates, caspase-8 activity was 280, 150, and 350% of that observed in control cells, respectively. No significant increase of caspase-8 activity was found in cells exposed for 8 h (Fig. 4, upper panel). At 5, 8, and 24 h of exposure, a higher (~150%) caspase-3 activity was also detected in cells, whereas no differences with respect to controls were found after 16 h exposure (Fig. 4, upper panel). A modest caspase-9 activation was observed only at prolonged times of exposure (16 and 24 h) and was followed by a late (24 h) caspase-3 activity increase (Fig. 4, upper panel). The rise of caspase-3 activity in cells exposed 24 h to the aggregates could be the effect of the activation of either the extrinsic and/or the intrinsic pathway; in addition, the previously reported activity of caspase-3 on procaspase-8 (31, 32) might explain the strong caspase-8 activation in these cells at 24 h.

In exposed NIH/3T3 cells, the pattern of caspase activation was quite different. An eightfold early increase of the caspase-9 activity was observed together with a much lower caspase-8 and caspase-3 activation at 5 h of exposure. At prolonged times of exposure, all three caspase activities declined toward control levels (Fig. 4, lower panel).

Role of Bid and mitochondria involvement

It is known that caspase-8-mediated cleavage of Bid may be a link between the extrinsic and the intrinsic pathways of apoptosis (15). Therefore, we investigated whether a proteolysis of Bid occurred in cells exposed to the HypF-N aggregates. Figure 5 shows a significant decrease of Bid both in H-END and NIH/3T3 cells exposed 5 and 8 h to the aggregates, whereas it rises again at higher times of exposure; this finding agrees with the similar extent of caspase-8 activation observed at 5 h in the two cell lines (Fig. 4). These data support the idea that the difference of the behavior of the two cell lines could rely, at least in part, on the early caspase-9 activation found in NIH/3T3 cells exposed to the aggregates. Therefore, we investigated the possible involvement of mitochondria in the aggregate-induced biochemical damage by checking the mitochondrial membrane potential in both cell lines.

Membrane depolarization was monitored by the uptake of 5,5′,6,6′-tetrachloro-1,1′,3,3′-tetraethylbenzimidazol-carbocyanine iodide (JC-1) leading to a shift in mitochondrial fluorescence from red to green. Exposed NIH/3T3 cells displayed a significant early mitochondrial membrane depolarization after 3 h exposure to the prefibrillar aggregates (Fig. 6E) that was maintained at longer times of exposure (Fig. 6F). This finding agrees with the early caspase-9 activation observed in this cell line. Most of the H-END cells displayed mitochondrial membrane depolarization only after 24 h exposure (Fig. 6C), whereas no significant

depolarization was observed at 3 h exposure to the aggregates (Fig. 6B), in agreement with the late caspase-9 activation found in this cell line. These data, together with the observed caspase-8-dependent proteolysis of Bid, suggest that mitochondrial injury is not the primary event of the apoptotic process in H-END cells but could be a late consequence of the activation of the extrinsic pathway.

Actually, when H-END cells were treated with a cell permeable caspase-8 specific inhibitor before the exposure to the HypF-N aggregates for 24 h, caspase-8 and caspase-9 activities were reduced by 36 and 28%, respectively (data not shown). Such caspase-9 activity reduction correlates with the disappearance of Bid cleavage during cell treatment with caspase-8 inhibitor (Fig. 7A). The decrease in caspase-8 activity on Bid makes it possible to observe an increase of Bid over control levels after cells treatment with HypF-N prefibrillar aggregates (Fig. 7A) that could be due to the up-regulation of the expression of the corresponding gene after p53 activation (33). Hence, we ascertained whether the p53 content was increased in exposed H-END cells.

The p53 pathway contributes to the apoptotic program in cells exposed to the aggregates

The possible involvement of p53 in H-END apoptosis was investigated by determining the p53 levels in cells exposed to the HypF-N aggregates together with the expression levels of two p53 targets, Bax and caspase-6. Western blot analysis reveals that all three proteins increased in the exposed cells with respect to controls, with apparent maxima at 5 h for p53 and caspase-6 and at 8 h for Bax (Fig. 7B). A similar behavior was displayed by Bid when caspase-8 was inhibited before cell exposure to the aggregates (Fig. 7A). This expression pattern suggests a contribution of the p53 pathway to H-END apoptosis triggered by the exposure to the HypF-N prefibrillar aggregates.

Intracellular ATP levels

To further support the idea that mitochondrial injury could explain the necrotic pattern observed in NIH/3T3, intracellular ATP levels were measured in both cell lines exposed 24 h to 2.0 μM aggregated or monomeric HypF-N. A 30% decrease in the ATP level with respect to controls was observed in NIH/3T3, whereas under the same conditions ATP levels in H-END cells were the same as in control cells (data not shown). The reduction of the ATP levels in NIH/3T3 cells could explain the finding that although these cells trigger the apoptotic program, as shown by the early activation of caspase-9 and 3, they are not able to complete it. This is indeed in agreement with previous reports indicating that the apoptotic program requires energy to proceed (34, 35).

DISCUSSION

We have previously reported that NIH/3T3 cells exposed to prefibrillar aggregates of HypF-N display impaired viability (6) and eventually die after early biochemical changes of intracellular free Ca^{2+} concentration and redox status (23). In this study, we have investigated in depth the biochemical features of cell death in two cell lines that undergo apoptosis (H-END) or necrosis (NIH/3T3) upon exposure to the HypF-N aggregates.

It is generally believed that cell death associated with protein aggregates is a result of the stimulation of the apoptotic response (14, 16, 36, 37). This seems to be the case for misfolded

variants of proteins, such as α-lactalbumin or Aβ$_{1-42}$, that are able to trigger apoptosis specifically in tumor (38) or neuronal (36) cells, respectively. Other recent data, however, suggest that Aβ$_{1-40}$ stimulates cell death both in culture (PC12) and in vivo (brain) via a necrotic rather than an apoptotic pathway (17–19, 39). Alternatively, when both processes occur, either a relatively small population of dying cells undergo apoptosis (17, 18) or cells die by secondary necrosis, a sequential event in the development of apoptosis in vitro (15, 16).

Recent data point to derangement of ion homeostasis and oxidative stress as key event underlying cell death in cells exposed to toxic protein aggregates (10, 11, 40–45). These data are reinforced by recent findings indicating that caspase-3 can cleave the plasma membrane Ca^{2+}-ATPase (46), the loss of function of which during apoptosis results in Ca^{2+} overload and secondary cell lysis or necrosis (15). Our results agree with these data, since, after an initial increase of caspases activity, necrosis appears to be the dominant feature of death in NIH/3T3 cells.

The pattern of caspase activation in the two investigated cell lines exposed to the aggregates is consistent with their different fate. In H-END cells, a remarkable activation of caspase-8 and a less pronounced activation of caspase-3 were found. In both cases, the activation was biphasic, displaying minima in cells exposed 8 (caspase-8) or 16 (caspase-3) h; caspase-9 activation occurred later and was only found in cells exposed 16 and 24 h. As caspase-3 is an effector caspase, downstream to caspase-8 and caspase-9, this pattern is consistent with an initial activation of caspase-3 by caspase-8 followed by a reactivation by caspase-8 and caspase-9 at later times of exposure. Since caspase-3 can activate caspase-8 (31, 32), the second wave of caspase-8 activity could represent a positive feedback arising from the initial caspase-3 activation. Our findings agree with recent data showing that Chinese hamster V79 cells and human K562 cells exposed 20 h to aggregates of an 11-Ala peptide display increased caspase-8 and caspase-3 activities before the apoptotic outcome (47).

Apparently, under these conditions, the extrinsic and the intrinsic pathways of apoptosis are activated in H-END cells, in agreement with previous findings showing that the aggregates are able to interact with the plasma membrane and to translocate into the cytosol (23) where they can interact with other organelles. Previously, it was reported that a molecular link, relying on the production of a truncated form of Bid, does exist between the extrinsic and the intrinsic pathway of apoptosis (48–50). The product of Bid cleavage by caspase-8 (tBid) translocates to the mitochondria where it induces oligomerization and insertion of Bax and/or Bak into the outer membrane; the subsequent membrane permeabilization (51) releases to the cytosol death-promoting factors such as cytochrome *c*, with apoptosome formation and caspase-9 activation (52).

Actually, in H-END cells exposed to the aggregates, we found a significant decrease of Bid and hence, presumably, an increase of its cleaved form. Such a decrease reached the maximum at 8 h exposure, possibly after the preceding caspase-8 activation; in the presence of the cell-permeable caspase-8 inhibitor, the decrease of Bid was not found. Taken together, our results support the hypothesis of a cross-talk between the extrinsic and intrinsic pathway in exposed H-END cells. In fact, the appearance of caspase-9 activity at later times of exposure to preaggregates in H-END cells suggests it follows caspase-8 activation via Bid cleavage. Coherently, the reduction in caspase-8 activation coming from pretreatment with the caspase-8 inhibitor results in a

diminished caspase-9 activity.

In this contest, the Bax increase in cells exposed 8 h to HypF-N preaggregates would favor the subsequent caspase-9 activation, interacting with tBid to promote the mitochondrial membrane permeabilization. The increase of Bax in exposed H-END cells suggests that p53 may contribute to the overall apoptotic pathway. Recent papers have reported that p53 and Bax are activated in cells microinjected with $A\beta_{1-42}$ (36) and that p53 is activated in cells affected by differing cellular stresses, supporting its role as apoptosis trigger by transcriptional induction of a wide network of target genes (53, 33). In addition to *Bax*, *Bid* is also transcriptionally regulated by p53 in response to stress stimuli such as γ-irradiation (33).

The levels of either p53 or of two p53-upregulated gene products, Bax and caspase-6, further support the involvement of the p53 pathway in the apoptosis of exposed H-END cells. In fact, the content of p53 increased sharply in cells exposed 5 h to the aggregates but progressively declined at longer times of exposure. Accordingly, the content of Bax, and, to a lesser extent, of caspase-6, increased at 5-8 h of exposure; moreover, an increase of Bid was observed when caspase-8 was inhibited. An increase of caspase-6 activity in human neurons committed to apoptosis in AD brains has previously been reported, supporting the idea that caspase-6 is involved in apoptosis of primary cultures of human neurons (54). Altogether, our data suggest the participation of p53 to the apoptotic program triggered in H-END cells exposed to the aggregates.

Our data may also contribute to explaining why NIH/3T3 cells are not able to support the initially triggered apoptotic program and eventually die by necrosis (or by secondary necrosis). Figure 4 shows that, in these cells, caspase-9 undergoes strong early, though not sustained, activation. The comparison of the patterns of caspase activation in NIH/3T3 and H-END cells shows that, while both undergo similar caspase-8 and caspase-3 activation and similar proteolysis of Bid at 5 h and 8 h exposure, the early and strong caspase-9 activation is found only in NIH/3T3. Such a strong activation agrees with the significant mitochondrial membrane depolarization in these cells exposed 3 h to the aggregates; instead, at the same time of exposure, no significant mitochondrial membrane depolarization was observed in H-END cells, where mitochondrial damage was found only at 24 h exposure, in agreement with the late caspase-9 activation.

These data suggest that the mitochondrial injury is not the primary event of the apoptotic process in H-END cells, but it can follow the activation of the extrinsic pathway possibly elicited by preaggregate interaction with the plasma membrane. Other triggers of the extrinsic pathway cannot be ruled out: in various cell lines an induction by p53 of the CD95 death receptor expression has been shown (55, 56). Moreover, a ligand-independent activation of Fas by ultraviolet radiation, cytotoxic drugs, or ROS was reported (57–59). Finally, the disruption of lipid rafts leads to a spontaneous clustering of Fas in the nonraft compartment of plasma membrane, with subsequent activation of caspase-8 and apoptosis (60).

NIH/3T3 cells seem to experience a primary activation of the intrinsic pathway, as indicated by the early onset of caspase-9 activity. The differing mitochondria involvement in cell death in either cell line is confirmed by the measurements of the ATP content in NIH/3T3 and H-END cells exposed 24 h to the aggregates. A sharp reduction of the energy load was found only in NIH/3T3 cells, confirming the heavier mitochondrial damage in these cells and providing a

possible clue to explain their inability to support the initially triggered apoptotic program. In fact, it is known that apoptosis requires high energy levels and that the same are dissipated during necrosis (34, 35). Evidence that cells targeted to apoptosis are forced to die by necrosis when intracellular ATP is depleted has previously been reported (35). A stronger and earlier mitochondrial injury could explain ATP depletion and the consequent necrotic degeneration observed in NIH/3T3 cells. A possibility is that the early increase of free Ca^{2+} and ROS previously reported in exposed NIH/3T3 cells (23) may be responsible of the early mitochondria involvement. It is known that free Ca^{2+} can interact with cardiolipin, to which cytochrome *c* is anchored; such a binding and/or cardiolipin oxidation favor cytochrome *c* release with the subsequent caspase-9 and caspase-3 activation (15). A large body of data supports the idea that the point of no return in cell necrosis depends on the loss of function of mitochondria (61) after the opening of the permeability transition pore triggered by the accumulation of Ca^{2+}, with subsequent outer membrane depolarization (61). Our data agree with these findings in that, at short times of exposure to the aggregates of the NIH/3T3, mitochondria appear to be heavily affected, as shown by the mitochondrial membrane depolarization and the early massive increase of caspase-9 that is released from mitochondria during the Ca^{2+}-mediated permeability transition.

Our data, together with those previously reported (23), support the existence, at least in most cases, of a common mechanism of aggregate toxicity to cells regardless of the origin and amino acid sequence of the aggregated polypeptide. This seems to proceed through free Ca^{2+} and ROS increases and activation of the apoptotic extrinsic pathway followed, when possible, by the intrinsic pathway. Our data also indicate that the different choices between apoptosis and necrosis could depend on the timing and severity of mitochondria derangement.

REFERENCES

1. Stefani, M., and Dobson, C. M. (2003) Protein aggregation and aggregate toxicity: new insights into protein folding, misfolding diseases and biological evolution. *J. Mol. Med.* **81,** 678–699

2. Dobson, C. M. (2003) Protein folding and misfolding. *Nature* **426,** 884–890

3. Selkoe, D. J. (2003) Folding proteins in fatal ways. *Nature* **426,** 900–904

4. Cohen, F. E., and Kelly, J. W. (2003) Therapeutic approaches to protein-misfolding diseases. *Nature* **426,** 905–909

5. Kayed, R., Head, E., Thompson, J. L., McIntire, T. M., Milton, S. C., Cotman, C. W., and Glabe, C. G. (2003) Common structure of soluble amyloid oligomers implies common mechanism of pathogenesis. *Science* **300,** 486–489

6. Bucciantini, M., Giannoni, E., Chiti, F., Baroni, F., Formigli, L., Zurdo, J., Taddei, N., Ramponi, G., Dobson, C. M., and Stefani, M. (2002) Inherent toxicity of aggregates implies

a common mechanism for protein misfolding diseases. *Nature* **416,** 507–511

7. Caughey, B., and Lansbury, P. T. (2003) Protofibrils, pores, fibrils, and neurodegeneration: separating the responsible protein aggregates from the innocent bystanders. *Annu. Rev. Neurosci.* **26,** 267–298

8. Walsh, D. M., and Selkoe, D. J. (2004) Oligomers on the brain: the emerging role of soluble protein aggregates in neurodegeneration. *Protein Pept. Lett.* **11,** 213–228

9. Mattson, M. P. (1999) Impairment of membrane transport and signal transduction systems by amyloidogenic proteins. *Methods Enzymol.* **309,** 733–768

10. Kruman, I. I., Pedersen, W. A., Springer, J. E., and Mattson, M. P. (1999) ALS-linked Cu/Zn-SOD mutation increases vulnerability of motor neurons to excitotoxicity by a mechanism involving increased oxidative stress and perturbed calcium homeostasis. *Exp. Neurol.* **160,** 28–39

11. Kawahara, M., Kuroda, Y., Arispe, N., and Rojas, E. (2000) Alzheimer's β-amyloid, human islet amylin, and prion protein fragment evoke intracellular free calcium elevations by a common mechanism in a hypothalamic GnRH neuronal cell line. *J. Biol. Chem.* **275,** 14077–14083

12. Bhatia, R., Lin, H., and Lal, R. (2000) Fresh and globular amyloid β protein(1-42) induces rapid cellular degeneration: evidence for AβP-channel-mediated cellular toxicity. *FASEB J.* **14,** 1233–1243

13. Butterfield, A. D., Drake, J., Pocernich, C., and Castegna, A. (2001) Evidence of oxidative damage in Alzheimer's disease brain: central role for amyloid β-peptide. *Trends Mol. Med.* **7,** 548–554

14. Ross, C. A. (2002) Polyglutamine pathogenesis: emergence of unifying mechanisms for Huntington's disease and related disorders. *Neuron* **35,** 819–822

15. Orrenius, S., Zhivotovsky, B., and Nicotera, P. (2003) Regulation of cell death: the calcium-apoptosis link. *Nat. Rev. Mol. Cell Biol.* **4,** 552–565

16. Watt, J. A., Pike, C. J., Walencewicz-Wasserman, A. J., and Cotman, C. W. (1994) Ultrastructural analysis of beta-amyloid-induced apoptosis in cultured hippocampal neurons. *Brain Res.* **661,** 147–156

17. Lane, N. J., Balbo, A., Fukuyama, R., Rapoport, S. I., and Galdzick, Z. (1998) The ultrastructural effects of beta-amyloid peptide on cultured PC12 cells: changes in cytoplasmic and intramembranous features. *J. Neurocytol.* **27,** 707–718

18. Velez-Pardo, C., Arroyave, S. T., Lopera, F., Castano, A. D., and Jimenez Del Rio, M. (2001) Ultrastructure evidence of necrotic neural cell death in familial Alzheimer's disease brains bearing presenilin-1 E280A mutation. *J. Alzheimer Dis.* **3,** 409–415

19. Iijima, K., Liu, H.-P., Chiang, A.-S., Hearn, S. A., Konsolaki, M., and Zhong, Y. (2004) Dissecting the pathological effects of human Aβ40 and Aβ42 in *Drosophila*: a potential model for Alzheimer's disease. *Proc. Natl. Acad. Sci. USA* **101,** 6623–6628

20. Tan, S., Schubert, D., and Maher, P. (2001) Oxytosis: a novel form of programmed cell death. *Curr. Top. Med. Chem.* **1,** 497–506

21. Nicotera, P., and Melino, G. (2004) Regulation of the apoptosis-necrosis switch. *Oncogene* **12,** 2757–2765

22. Fändrich, M., and Dobson, C. M. (2002) The behaviour of polyamino acids reveals an inverse side chain effect in amyloid structure formation. *EMBO J.* **21,** 5682–5690

23. Bucciantini, M., Calloni, G., Chiti, F., Formigli, L., Nosi, D., Dobson, C. M., and Stefani, M. (2004) Pre-fibrillar amyloid protein aggregates share common features of cytotoxicity. *J. Biol. Chem.* **279,** 31374–31382

24. Yang, W., Dunlap, J. R., Andrews, R. B., and Wetzel, R. (2002) Aggregated polyglutamine peptides delivered to nuclei are toxic to mammalian cells. *Hum. Mol. Genet.* **11,** 2905–2917

25. Kranenburg, O., Kroon-Batenburg, L. M. J., Reijerkerk, A., Wu, Y.-P., Voest, E. E., and Gebbink, M. F. (2003) Recombinant endostatin forms amyloid fibrils that bind and are cytotoxic to murine neuroblastoma cells in vitro. *FEBS Lett.* **539,** 149–155

26. Kelly, J. W., and Balch, E. W. (2003) Amyloid as a natural product. *J. Cell Biol.* **161,** 461–462

27. Gebbink, M. F., Voest, E. E., and Reijerkerk, A. (2004) Do antiangiogenic protein fragments have amyloid properties? *Blood* **104,** 1601–1605

28. Chiti, F., Bucciantini, M., Capanni, C., Taddei, N., Dobson, C. M., and Stefani, M. (2001) Solution conditions can promote formation of either amyloid protofilaments or mature fibrils from the HypF N-terminal domain. *Protein Sci.* **10,** 2541–2547

29. Fadok, V. A., Voelker, D. R., Campbell, P. A., Cohen, J. J., Bratton, D. L., and Henson, P. M. (1992) Exposure of phosphatidylserine on the surface of apoptotic lymphocytes triggers specific recognition and removal by macrophages. *J. Immunol.* **148,** 2207–2216

30. Martin, S. J., Reutelingsperger, C. P., McGahon, A. J., Rader, J. A., van Schie, R. C., LaFace, D. M., and Green, D. R. (1995) Early redistribution of plasma membrane phosphatidylserine is a general feature of apoptosis regardless of the initiating stimulus: inhibition by overexpression of Bcl-2 and Abl. *J. Exp. Med.* **182,** 1545–1556

31. Slee, E. A., Harte, M. T., Kluck, R. M., Wolf, B. B., Casiano, C. A., Newmeyer, D. D., Wang, H. G., Reed, J. C., Nicholson, D. W., Alnemri, E. S., et al. (1999) Ordering the cytochrome c-initiated caspase cascade: hierarchical activation of caspases-2, -3, -6, -7, -8, and -10 in a caspase-9-dependent manner. *J. Cell Biol.* **144,** 281–292

32. Pirnia, F., Schneider, E., Betticher, D. C., and Borner, M. M. (2002) Mitomycin C induces

apoptosis and caspase-8 and -9 processing through a caspase-3 and Fas-independent pathway. *Cell Death Differ.* **9,** 905–914

33. Haupt, S., Berger, M., Goldberg, Z., and Haupt, Y. (2003) Apoptosis − the p53 network. *J. Cell Sci.* **116,** 4077–4085

34. Richter, C., Schweizer, M., Cossarizza, A., and Franceschi, C. (1996) Control of apoptosis by the cellular ATP level. *FEBS Lett.* **378,** 107–110

35. Leist, M., Single, B., Castoldi, A. F., Kuhnle, S., and Nicotera, P. (1997) Intracellular adenosine triphosphate (ATP) concentration: a switch in the decision between apoptosis and necrosis. *J. Exp. Med.* **185,** 1481–1486

36. Zhang, Y., McLaughlin, R., Goodyerm, C., and LeBlanc, A. (2002) Selective cytotoxicity of intracellular amyloid β peptide$_{1-42}$ through p53 and Bax in cultured primary human neurons. *J. Cell Biol.* **156,** 519–529

37. Morishima, Y., Gotoh, Y., Zieg, J., Barrett, T., Takano, H., Flavell, R., Davis, R. J., Shirasaki, Y., and Greenberg, M. E. (2001) Beta-amyloid induces neuronal apoptosis via a mechanism that involves the c-Jun N-terminal kinase pathway and the induction of Fas ligand. *J. Neurosci.* **21,** 7551–7560

38. Svanborg, C., Agerstam, H., Aronson, A., Bjerkvig, R., Duringer, C., Fischer, W., Gustafsson, L., Hallgren, O., Leijonhuvud, I., Linse, S., et al. (2003) HAMLET kills tumor cells by an apoptosis-like mechanism-cellular, molecular, and therapeutic aspects. *Adv. Cancer Res.* **88,** 1–29

39. Bhagat, Y. A., Obenaus, A., Richardson, J. S., and Kendall, E. J. (2002) Evolution of β-amyloid induced neuropathology: magnetic resonance imaging and anatomical comparisons in the rodent hippocampus. *MAGMA* **14,** 223–232

40. Kourie, J. I., and Henry, C. L. (2002) Ion channel formation and membrane-linked pathologies of misfolded hydrophobic proteins: the role of dangerous unchaperoned molecules. *Clin. Exp. Pharmacol. Physiol.* **29,** 741–753

41. Squier, T. C. (2001) Oxidative stress and protein aggregation during biological aging. *Exp. Gerontol.* **36,** 1539–1550

42. Milhavet, O., and Lehmann, S. (2002) Oxidative stress and the prion protein in transmissible spongiform encephalopathies. *Brain Res. Rev.* **38,** 328–339

43. Hyun, D.-H., Lee, M. H., Hattori, N., Kubo, S.-I., Mizuno, Y., Halliwell, B., and Jenner, P. (2002) Effect of wild-type or mutant parkin on oxidative damage, nitric oxide, antioxidant defenses, and the proteasome. *J. Biol. Chem.* **277,** 28572–28577

44. Mattson, M. P., and Liu, D. (2002) Energetics and oxidative stress in synaptic plasticity and neurodegenerative disorders. *Neuromolecular Med.* **2,** 215–231

45. Ferreiro, E., Oliveira, C. R., and Pereira, C. (2004) Involvement of endoplasmic reticulum

Ca^{2+} release through ryanodine and inositol 1,4,5-triphosphate receptors in the neurotoxic effects induced by the amyloid-beta peptide. *J. Neurosci. Res.* **76,** 872–880

46. Schwab, B. L., Guerini, D., Didszun, C., Bano, D., Ferrando-May, E., Fava, E., Tam, J., Xu, D., Xanthoudakis, S., Nicholson, D. W., et al. (2002) Cleavage of plasma membrane calcium pumps by caspases: a link between apoptosis and necrosis. *Cell Death Differ.* **9,** 818–831

47. Giri, K., Ghosh, U., Bhattacharyya, N. P., and Basak, S. (2003) Caspase 8 mediated apoptotic cell death induced by β-sheet forming polyalanine peptides. *FEBS Lett.* **555,** 380–384

48. Li, H., Zhu, H., Xu, C. J., and Yuan, J. (1998) Cleavage of BID by caspase 8 mediates the mitochondrial damage in the Fas pathway of apoptosis. *Cell* **94,** 491–501

49. Korsmeyer, S. J., Wei, M. C., Saito, M., Weiler, S., Oh, K. J., and Schlesinger, P. H. (2000) Pro-apoptotic cascade activates BID, which oligomerizes BAK or BAX into pores that result in the release of cytochrome c. *Cell Death Differ.* **7,** 1166–1173

50. Esposti, M. D. (2002) The roles of Bid. *Apoptosis* **7,** 433–440

51. Akhtar, R. S., Ness, J. M., and Roth, K. A. (2004) Bcl-2 family regulation of neuronal development and neurodegeneration. *Biochim. Biophys. Acta* **1644,** 189–203

52. Saelens, X., Festjens, N., Walle, L. V., van Gurp, M., van Loo, G., and Vandenabeele, P. (2004) Toxic proteins released from mitochondria in cell death. *Oncogene* **23,** 2861–2874

53. Schuler, M., and Green, D. R. (2001) Mechanisms of p53-dependent apoptosis. *Biochem. Soc. Trans.* **29,** 684–688

54. Leblanc, A., Liu, H., Goodyer, C., Bergeron, C., and Hammond, J. (1999) Caspase-6 role in apoptosis of human neurons, amyloidogenesis, and Alzheimer's disease. *J. Biol. Chem.* **274,** 23426–23436

55. Muller, M., Wilder, S., Bannasch, D., Israeli, D., Lehlbach, K., Li-Weber, M., Friedman, S. L., Galle, P. R., Stremmel, W., Oren, M., et al. (1998) p53 activates the CD95 (APO-1/Fas) gene in response to DNA damage by anticancer drugs. *J. Exp. Med.* **188,** 2033–2045

56. Gutierrez del Arroyo, A., Gil-Lamagniere, C., Lazaro, I., de Marco, M. C., Layunta, I., and Silva, A. (2000) Involvement of p53 and interleukin 3 in the up-regulation of CD95 (APO-1/Fas) by X-ray irradiation. *Oncogene* **19,** 3647–3655

57. Aragane, Y., Kulms, D., Metze, D., Wilkes, G., Poppelmann, B., Luger, T. A., and Schwarz, T. (1998) Ultraviolet light induces apoptosis via direct activation of CD95 (Fas/APO-1) independently of its ligand CD95L. *J. Cell Biol.* **140,** 171–182

58. Micheau, O., Solary, E., Hammann, A., and Dimanche-Boitrel, M. T. (1999) Fas ligand-dependent, FADD-mediated activation of the Fas death pathway by anticancer drugs. *J. Biol. Chem.* **274,** 7987–7992

59. Huang, H. L., Fang, L. W., Lu, S. P., Chou, C. K., Luh, T. Y., and Lai, M. Z. (2003) DNA-damaging reagents induce apoptosis through reactive oxygen species-dependent Fas aggregation. *Oncogene* **22,** 8168–8177

60. Gniadecki, R. (2004) Depletion of membrane cholesterol causes ligand-independent activation of Fas and apoptosis. *Biochem. Biophys. Res. Commun.* **320,** 165–169

61. Ferrari, D., Pinton, P., Szabadakai, G., Chiami, M., Campanella, M., Pozzan, T., and Rizzuto, R. (2002) Endoplasmic reticulum, Bcl-2 and Ca^{2+} handling in apoptosis. *Cell Calcium* **32,** 413–420

Fig. 1
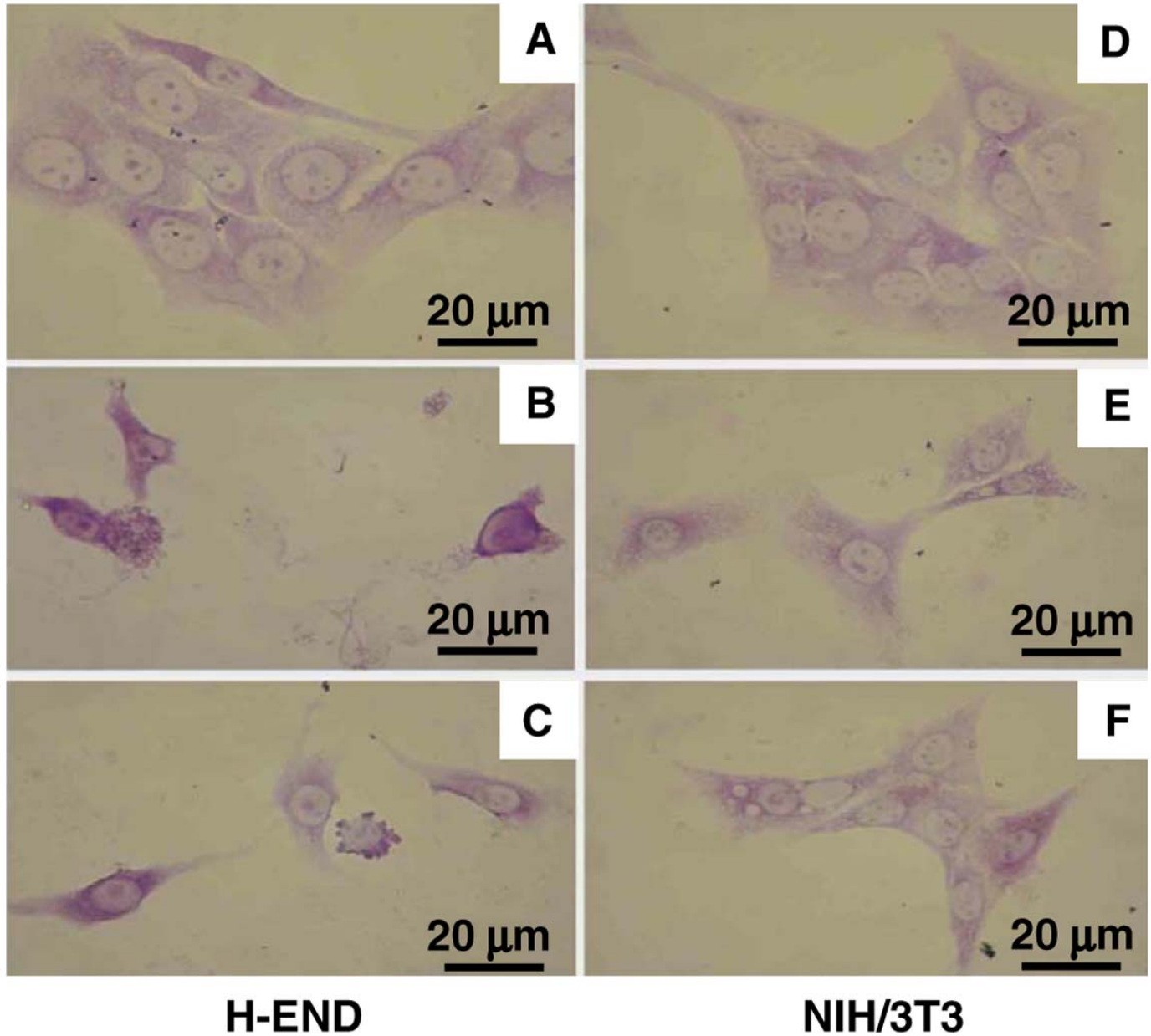
Figure 1. Light microscopic examination of haematoxylin/eosin stained H-END and NIH/3T3 cells 24 h exposed to the toxic HypF-N prefibrillar aggregates (10 μM). Cells grown on glass cover slips were 24h exposed to 10 μM soluble HypF-N or 10μM prefibrillar aggregates of HypF-N added to culture medium. Cell morphology was observed by haematoxylin/eosin staining and light microscopy examination. *A* and *D*) Control cells exposed for 24 h to 10 μM soluble HypF-N. *B, C, E,* and *F*) Cells exposed for 24 h to 10 μM prefibrillar aggregates of HypF-N.

Fig. 2
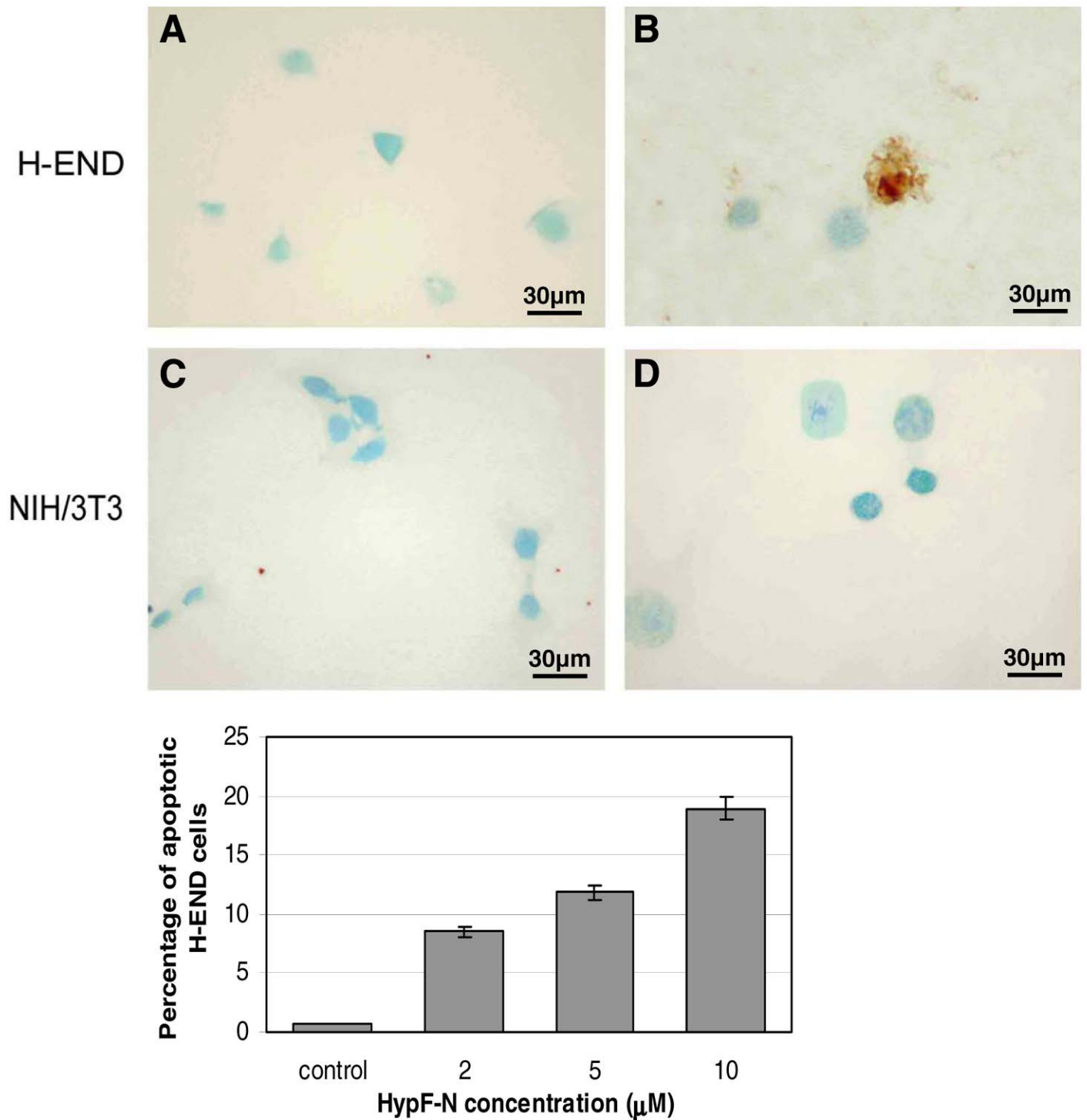
Figure 2. Apoptosis determination with Klenow FragEL™ DNA fragmentation detection Kit (ISEL assay). Photos: DNA fragmentation was detected by in situ end labeling (ISEL) technique of nicked DNA. Counterstaining was performed with methyl green. Cells were 24 h exposed to 10 µM soluble HypF-N (controls) or 10 µM prefibrillar aggregates added to culture medium. *A* and *C*) control cells; *B* and *D*) treated cells. Graph: Dose-dependent effect of prefibrillar HypF-N aggregates on percentage of apoptotic H-END cells after 24 h treatment. Control is treatment with 10 µM soluble HypF-N. Count of apoptotic nuclei was performed by light microscopy observation of cells stained with Klenow FragEL Kit. Four representative fields containing ~50 cells were analyzed. Data are means ± SD of 2 distinct experiments.

Fig. 3
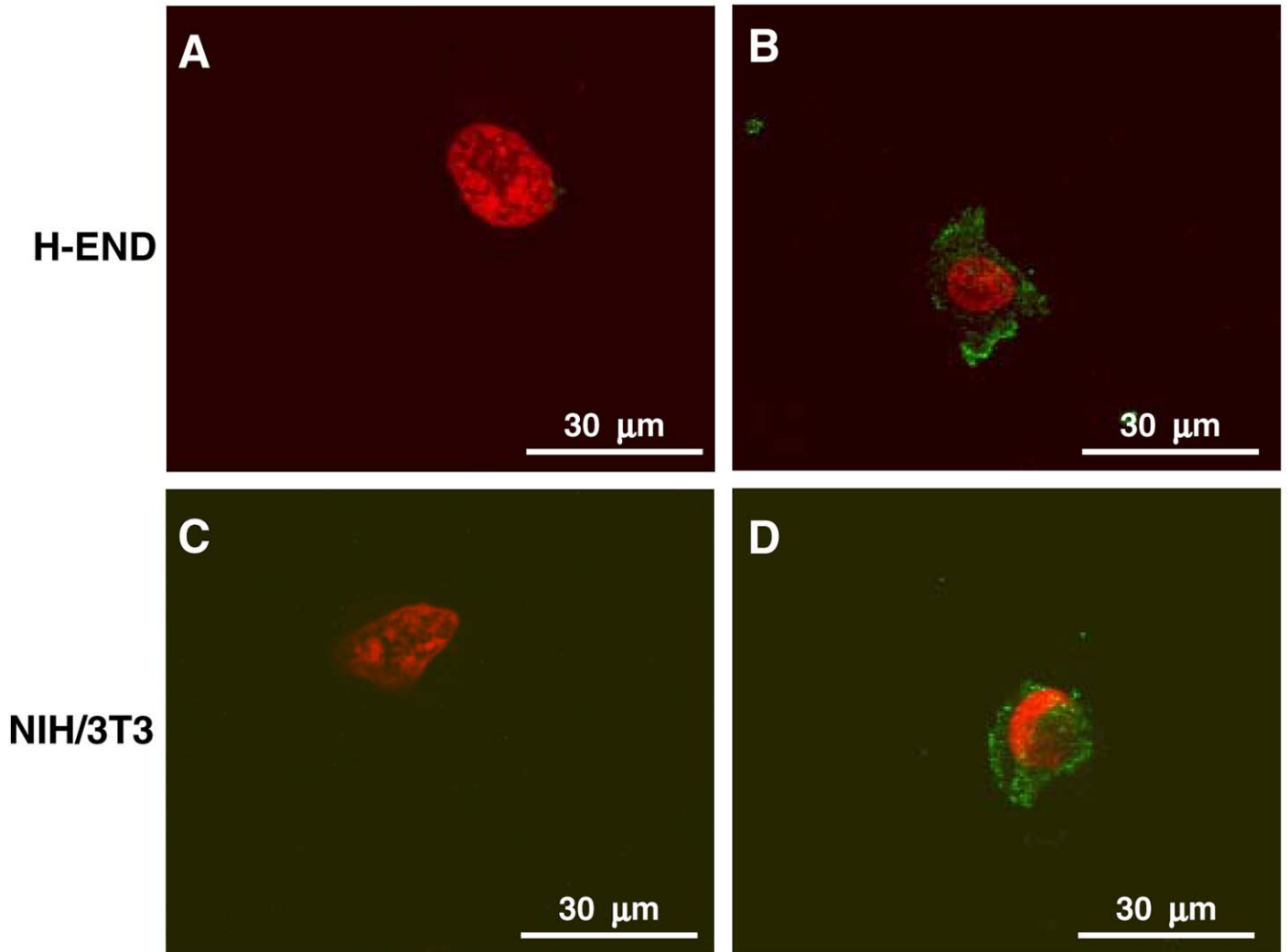
Figure 3. Annexin V-FITC binding to H-END and NIH/3T3 cells after 24 h exposure to the HypF-N prefibrillar aggregates (2 μM). Cellular nuclei were stained in red with propidium iodide (PI). Fluorescein isothiocyanate (FITC)-conjugated annexin V binds to phosphatidylserine exposed to the outer surface of the plasma membrane during early stages of apoptosis. *A* and *C*) Control H-END (*A*) or NIH/3T3 (*C*) cells exposed for 24 h to 2.0 μM soluble HypF-N. *B* and *D*) H-END (*B*) or NIH/3T3 (*D*) cells exposed for 24 h to 2.0 μM prefibrillar HypF-N.

Fig. 4
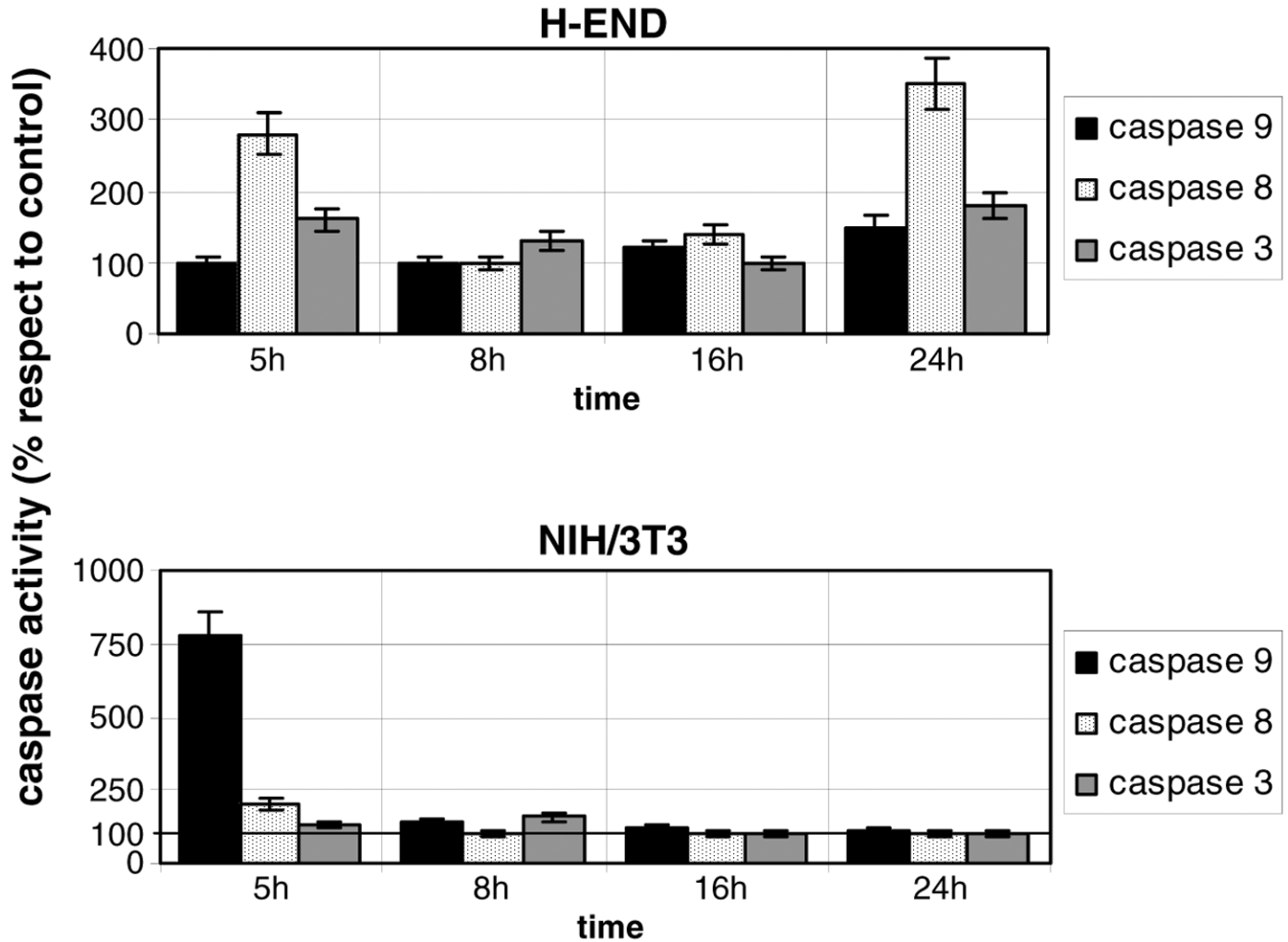
Figure 4. Time course of caspase activity in H-END and NIH/3T3 cells after incubation with 2.0 µM toxic HypF-N prefibrillar aggregates. Caspase-9 activity was determined incubating cellular lysates for 2 h at 37°C in the presence of 50 µM Ac-LEHD-AMC. Caspase-3 and -8 activities were determined incubating for 4h at 37°C in the presence of 200 µM Ac-DEVD-pNA and 200 µM Ac-IETD-pNA respectively. Values are means ± SD of 3 replicates and are expressed as percent respect to values found in control cells (100%) treated with 2 µM soluble HypF-N for corresponding intervals of time. These data come from 1 experiment out of 10, which gave qualitatively identical results.

Fig. 5
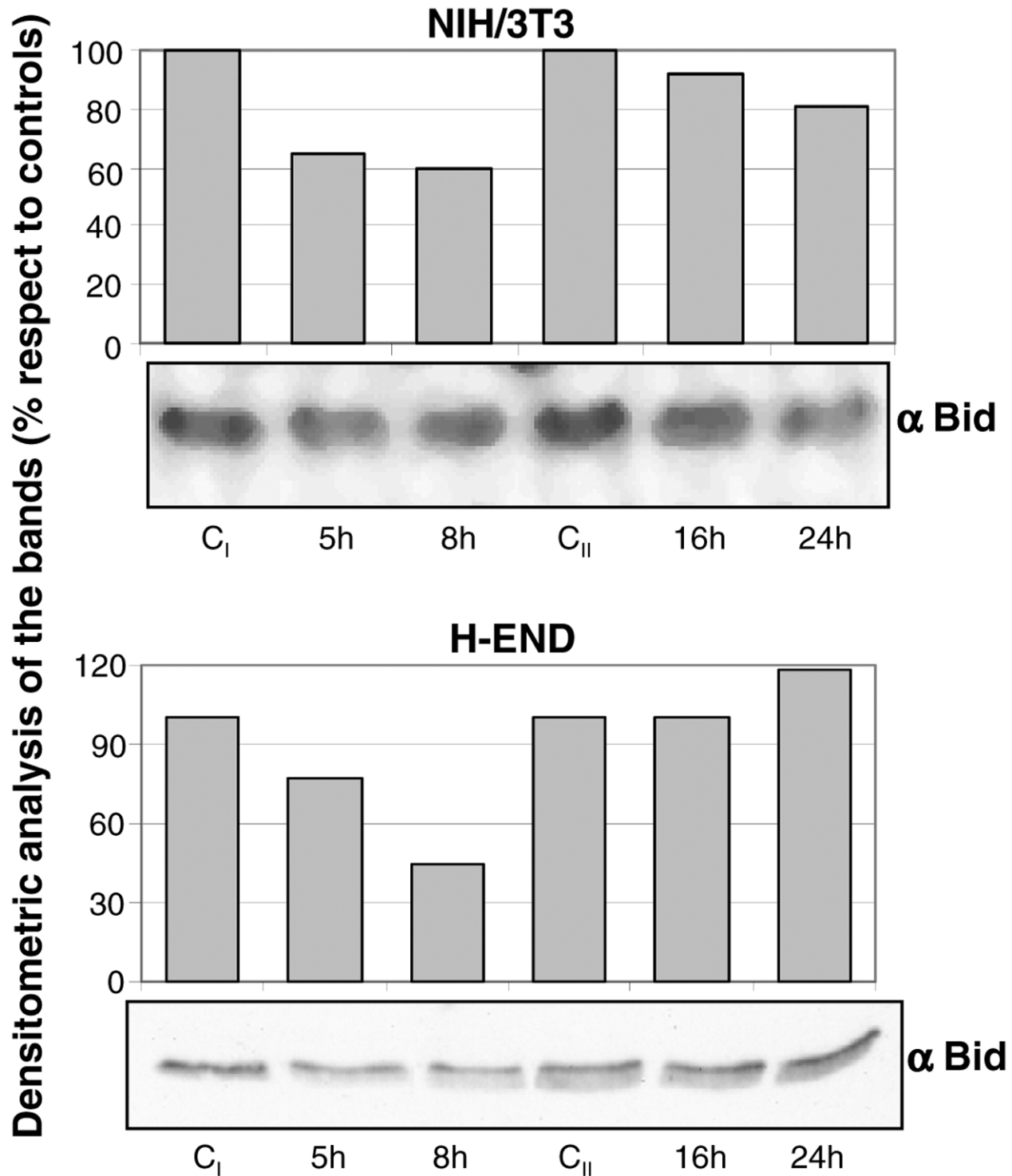
Figure 5. Analysis of Bid levels. Cells were treated for short time intervals (5 h, 8 h) or long time intervals (16 h, 24 h) with 2 μM HypF-N prefibrillar aggregates. Controls (C_I for short and C_{II} for long time intervals) were treated with 2.0 μM soluble protein. Cell lysates were obtained and equal protein amounts subjected to 15% SDS-PAGE and Western blotting with anti-Bid antibodies. Densitometric analysis of bands was performed using QuantiScan software. Histograms are intensity of bands when controls were made 100%. This is a representative experiment out of 5 that gave qualitatively identical results.

Fig. 6
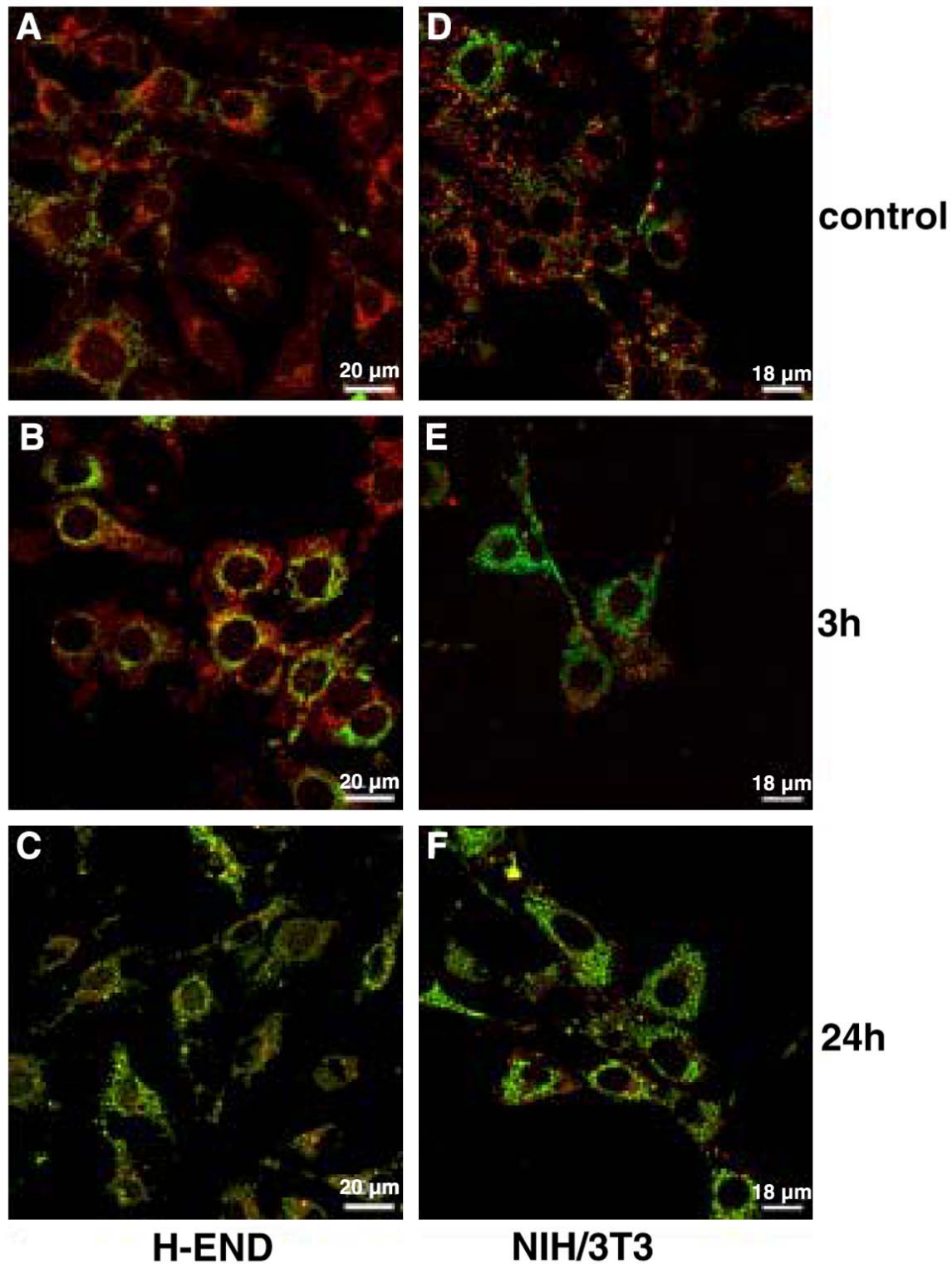
Figure 6. JC-1 analysis of mitochondrial membrane potential ΔΨ$_M$ in H-END and NIH/3T3 cells. Change in ΔΨ$_M$ was detected by a fluorescence-based assay. For experimental details, see Materials and Methods. **_Left panels_**: H-END cells. **_Right panels_**: NIH/3T3 cells. **_A_** and **_D_**) Control cells exposed 24 h to 2.0 μM soluble HypF-N. **_B_** and **_E_**) Cells exposed for 3 h to 2.0 μM HypF-N prefibrillar aggregates. **_C_** and **_F_**) Cells exposed for 24 h to 2.0 μM prefibrillar aggregates of HypF-N.

Fig. 7
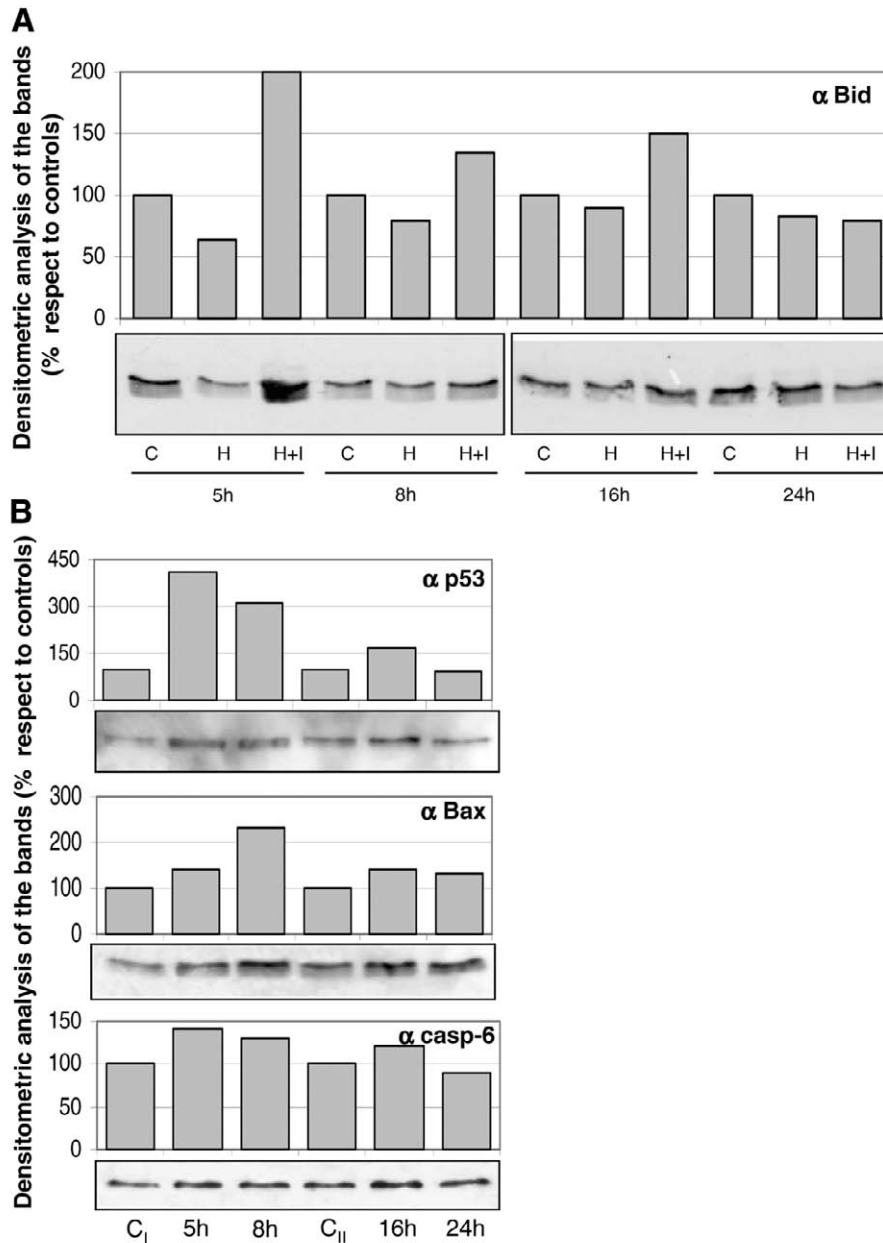
Figure 7. Analysis of p53 activation during H-END cells treatment with HypF-N prefibrillar aggregates. *A*) Analysis of Bid levels following caspase-8 inhibition**.** Cells were pretreated for 2 h with 10 µM cell permeable Ac-IETD-CHO prior to 2.0 µM HypF-N pre-fibrillar aggregates addition. Cells that did not receive the caspase-8 inhibitor received an equal amount of DMSO (vehicle). Cell lysates were obtained and equal protein amounts subjected to 15% SDS-PAGE and Western blotting with anti-Bid antibodies. This is a representative experiment out of three that gave qualitatively identical results. C: controls; H: treated with HypF-N prefibrillar aggregates; H+I*:* treated with caspase-8 inhibitor before HypF-N addition. *B*) Analysis of p53, Bax and caspase-6 level during H-END cells treatment with HypF-N prefibrillar aggregates. Cells were treated for short time intervals (5 h, 8 h) or long time intervals (16 h, 24 h) with 2 µM HypF-N prefibrillar aggregates. Controls (C_I for short and C_{II} for long time intervals) were treated with 2.0 µM soluble protein. Cell lysates were obtained and equal protein amounts subjected to 15% SDS-PAGE and Western blotting with anti-p53, anti-Bax or anti-caspase-6 antibodies. This is a representative experiment out of 5 that gave qualitatively identical results. Densitometric analysis of bands was performed using QuantiScan software. Histograms are intensity of bands considering controls as 100%.